INSTITUTE OF PHYSICS PUBLISHING JOURNAL OF PHYSICS: CONDENSED MATTER

J. Phys.: Condens. Matter **17** (2005) S201–S220 doi:10.1088/0953-8984/17/8/002

Theory of sum-frequency generation spectroscopy of adsorbed molecules using the density matrix method—broadband vibrational sum-frequency generation and applications

M Bonn[1,2], **H Ueba**[3,5] **and M Wolf**[4]

[1] FOM Institute for Atomic and Molecular Physics, Kruislaan 407, 1098 SJ Amsterdam, The Netherlands
[2] Leiden Institute of Chemistry, Leiden University, PO Box 9502, 2300 RA Leiden, The Netherlands
[3] Department of Electronics, Toyama University, Toyama 930-8550, Japan
[4] Institut fur Experimentalphysik, Freie Universitat Berlin, Arnimallee 14, 14195 Berlin, Germany

E-mail: ueba@eng.toyama-u.ac.jp

Received 8 July 2004, in final form 29 September 2004
Published 11 February 2005
Online at stacks.iop.org/JPhysCM/17/S201

Abstract

A generalized theory of frequency- and time-resolved vibrational sum-frequency generation (SFG) spectroscopy of adsorbates at surfaces is presented using the density matrix formalism. Our theoretical treatment is specifically aimed at addressing issues that accompany the relatively novel SFG approach using broadband infrared pulses. The ultrashort duration of these pulses makes them ideally suited for time-resolved investigations, for which we present a complete theoretical treatment. A second key characteristic of these pulses is their large bandwidth and high intensity, which allow for highly non-linear effects, including vibrational ladder climbing of surface vibrations. We derive general expressions relating the density matrix to SFG spectra, and apply these expressions to specific experimental results by solving the coupled optical Bloch equations of the density matrix elements. Thus, we can theoretically reproduce recent experimentally demonstrated hot band SFG spectra using femtosecond broadband infrared excitation of carbon monoxide (CO) on a Ru(001) surface.

(Some figures in this article are in colour only in the electronic version)

1. Introduction

Surface science has developed a broad spectrum of experimental techniques for studying and controlling the physical and chemical properties of surfaces with atomic precision. However,

[5] Author to whom any correspondence should be addressed.

many of these techniques are applicable only at the solid/vacuum interface, and not at ambient conditions or at buried (liquid/solid or solid/solid) interfaces. Furthermore, studies of surface dynamics often require high temporal resolution and molecular specificity to unravel the underlying elementary processes. In this context the non-linear optical technique of infrared (IR)–visible (VIS) surface sum-frequency generation (SFG) [1] has proven to be a very versatile tool in studying the structure and dynamics of molecules absorbed on surfaces and at interfaces (for a recent review, see [2]). SFG relies on the fact that for most materials, the second-order non-linear susceptibility $\chi^{(2)}$ is non-zero only at the surface. This makes it an ideal technique for studying molecules at surfaces and buried interfaces because of its selective sensitivity to the surface region and its high degree of molecular specificity: the foremost feature of this technique is its capability of monitoring intramolecular vibrations of molecules on the surface, essentially allowing one to look directly inside the molecular properties of the surface layer. In recent years the SFG technique has been extended to the use of broad bandwidth, femtosecond infrared laser pulses [6–15] and to two-dimensional (IR–VIS) double-resonant SFG spectroscopy [37, 38, 40, 4, 5, 3]. Here we will focus on the theory and recent applications of the femtosecond IR broadband approach, which removes the necessity of scanning the frequency of the infrared beam. Moreover, tunable infrared laser pulses with a duration down to $\sim$100 fs are ideally suited for time-resolved studies of vibrational and surface dynamics as well as surface reactions.

The essence of most of these time-resolved experiments is introducing a variable delay between the pulses: generally the system is brought out of equilibrium with an excitation ('pump') pulse, whereafter the return to equilibrium is monitored with a delayed ('probe') pulse (or pair of pulses) at different times after the pump pulse. Three kinds of time-resolved experiments involving SFG are depicted in figure 1. In the most elementary time-resolved SFG experiment (figure 1(b)), the SFG pulse pair (IR and VIS) are simply delayed with respect to each other (i.e. there is no pump pulse). With this technique, the IR pulse resonantly and coherently excites the vibrational polarization, and this coherence decays due to dephasing as $\exp(-t/T_2)$. When the duration of the visible pulse incident on the surface, delayed by t_d, is less than or comparable to T_2, it probes the remaining coherence. The decay of the frequency-integrated SFG signal is dictated by T_2. This coherence decay is the so-called *free induction decay* (FID). It is evident that frequency resolution is lost in this type of experiment, as the requirement that the duration of the visible pulse is less than T_2 dictates that—per definition—the spectral bandwidth of the visible pulse is too large to resolve the vibrational resonance.

Two experimental examples of these two kinds of measurements are presented in figure 2. Because the incident IR pulse is so short, its bandwidth is much larger than that of the vibrational resonance (left panel). In spite of that, the spectral components of the radiated SFG are determined by the linewidth of the resonance if the resonant polarization is upconverted with a temporally long, spectrally narrow VIS pulse. As a result, good frequency resolution can be obtained. In the time domain measurement, the VIS pulse is also short (and therefore spectrally broad), resulting in good time resolution but poor frequency resolution. Here, the spectrally integrated SFG signal is recorded as a function of delay time.

It should be noted that the decay time obtained from FID is equal to T_2 only in the absence of inhomogeneous broadening, as extensively discussed in [16]. Such time domain measurement of the polarization decay is equivalent to the information obtained with conventional frequency domain experiments, in which the coherence decay rate determines the linewidth. However, it has been shown that there are circumstances where either frequency or the time domain approach may be preferable, as will also be illustrated in more detail below [17].

A second class of time-resolved SFG measurements can be performed by introducing a third pulse, either an intense infrared pulse that excites vibrations in the adsorbate layer

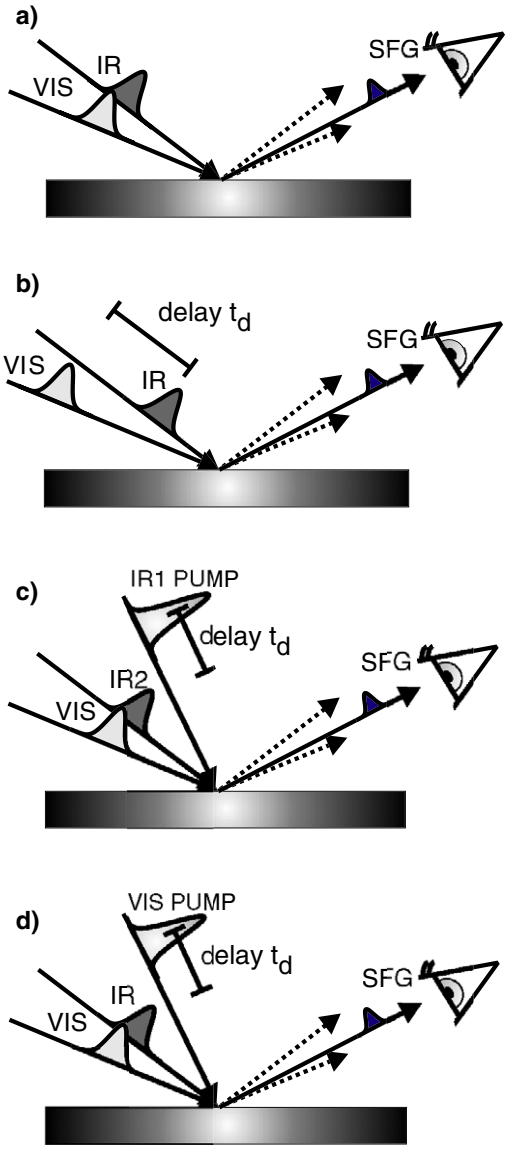

Figure 1. Pulse sequences of conventional (a) and time-resolved ((b)–(d)) SFG. (a) In a conventional SFG experiment, the infrared and visible pulses overlap in space and time on the surface, and the SFG light is radiated in the phase-matched direction. (b) The IR pulse resonantly excites the vibrational polarization in a coherent manner, and this coherence decays due to dephasing as $\exp(-t/T_2)$. When the delay of the visible pulse, t_d, is less than or comparable to T_2, it probes the remaining coherence. From the decay of the SFG signal, T_2 can be deduced. The decay of the coherent polarization induced by the IR pulse is the so-called *free induction decay* (FID). (c) An intense infrared pump pulse (IR1 tuned to the vibrational resonance at a surface) saturates the fundamental $v = 0 \rightarrow 1$ transition. After a certain time delay t_d, a pair (IR2 and visible) of weak probe pulses arrives at the surface. The output at sum frequency decays as a function of t_d with the population relaxation time T_1 of the excited state. (d) An intense (visible, or near-IR) pump pulse excites the (metal) substrate, which affects the vibration of adsorbates on the surface (for example by non-adiabatic coupling of hot substrate electrons with nuclear degrees of freedom of the adsorbate). The resulting time-dependent changes in the vibrations are monitored by a weak SFG probe pair.

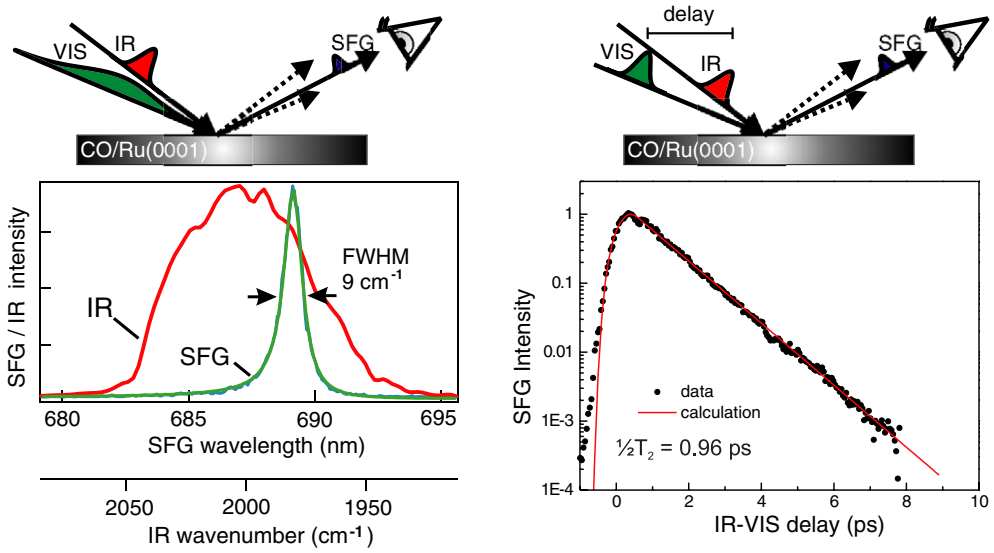

Figure 2. Two experimental examples for conventional (left panel) and time-resolved (right panel) broadband SFG. Left: in the frequency-resolved experiment, the bandwidth of the incident IR pulse is much larger than that of the vibrational resonance. The vibrational polarization, however, can only be built up significantly around the resonance. If the polarization is upconverted with a temporally long, spectrally narrow VIS pulse, good frequency resolution can be obtained. Right: in the time-resolved experiment, both incident pulses are short, and the spectrally integrated SFG signal is recorded as a function of delay time.

(figure 1(c)) [18–25], or an intense visible pulse that excites the underlying substrate (figure 1(d)) [9, 15, 26–31]. In the case of an infrared pump (figure 1(c)), this intense pulse (IR1) is tuned to a vibrational resonance at the surface, saturating the fundamental $v = 0 \rightarrow 1$ transition. After a certain time delay t_d, a pair (IR2 and visible) of weak probe pulses arrives at the surface. The output at the sum frequency decays as a function of t_d with a time constant determined by the recovery time of the ground state. If there is no intermediate state between the ground state and excited state probed, the recovery time of the ground state is equal to the population relaxation time T_1 of the excited state. A complete density matrix theory of such pump–probe SFG experiments for investigating the pump-induced change of the population between the ground and the excited state has been presented by Harris and Rothberg [32], and will not be pursued here. Experimentally, there is also the possibility of varying the IR pulse *energy* at fixed delay $t_d = 0$. If, moreover, the two infrared pulses are in a collinear geometry, this reduces the three-pulse experiment to a two-pulse experiment, and allows one to record SFG signals from the various higher lying vibrations on the vibrational lifetime. Such experiments also allow one to accurately determine the vibrational anharmonicity [10] and excited state linewidths [33], as well as the direct observation of energy delocalization due to dipole–dipole coupling [34, 35], as discussed below.

The density matrix formalism provides a theoretical framework for an adequate description of these different kinds of measurements, both in the frequency and the time domain. The elements of the time-dependent density matrix can be directly related to the population of the different resonant levels involved (diagonal elements), as well as the coherence between these levels (off-diagonal elements). The latter, for example, are directly proportional to the (non-linear) polarization that radiates the SFG field. Although for conventional SFG a

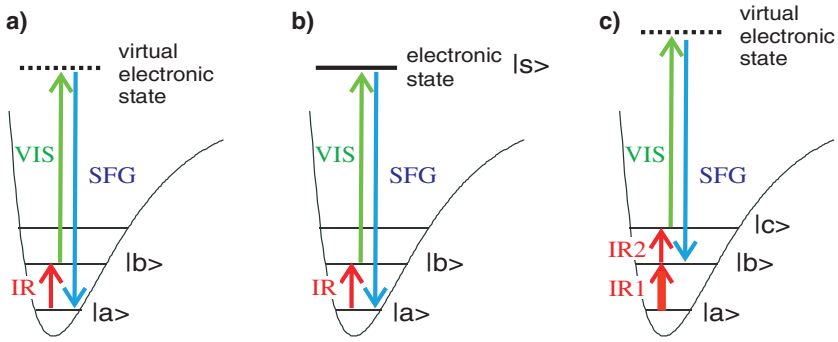

Figure 3. A schematic level diagram of different types of SFG spectroscopy, involving, respectively, two (panel (a)) and three (panels (b) and (c)) resonant levels. The situation in panel (b) corresponds to vibrationally and electronically (doubly) resonant SFG. Panel (c) depicts the case of SFG from higher lying states following excitation from the ground state.

description in terms of two levels (the vibrational ground and first excited state) suffices, this is not the case for many of the extended non-linear applications mentioned above. This is illustrated in figures 3(a)–(c), which shows the situation where the two-level description is appropriate, but also two examples for which a three-level description is essential. In the case of conventional IR–VIS vibrational SFG spectroscopy (figure 3(a)) the IR pulse resonantly excites the transition from the ground ($v = 0$) to the first excited ($v = 1$) state. The resulting polarization is upconverted by a spectrally narrow visible pulse, which is not resonant with a pronounced electronic transition or acts on a continuum of electronic states. On the other hand, if an electronic (panel (b)) or an additional vibrational resonance (panel (c)) is excited, the transitions to these levels have to be explicitly taken into account in the theoretical treatment using the density matrix method. For example, if an intense, broadband IR pulse saturates the fundamental transition ($v = 0 \rightarrow 1$), significant population is transferred to the ($v = 1$) state and the polarization induced at the ($v = 1 \rightarrow 2$) frequency gives rise to an additional hot band resonance in the SFG spectrum [10].

This paper is organized as follows. We first develop the general description of time-resolved SFG spectroscopy based on the density matrix formalism and briefly describe the experimental set-up. We then discuss applications to time-resolved SFG measurements of the free induction decay (FID), with particular emphasis on the influence of the pulse shape and lineshape analysis based on FID. Finally we analyse vibrational ladder climbing and excited state SFG spectroscopy with intense IR pulses.

2. Theory of SFG using the density matrix method: general approach

Consider a non-linear optical process in which a system, defined by the vibrational ground and excited states $|a\rangle$ and $|b\rangle$, and a (virtual) electronic state $|s\rangle$, interacts with an external infrared field $E_{\mathrm{IR}}(t)$ and a visible field $E_{\mathrm{VIS}}(t)$ as illustrated in figure 3(a). The total Hamiltonian of the system is given by

$$H = H_0 + H', \tag{1}$$

where H_0 is the material Hamiltonian characterized by

$$H_0|\alpha\rangle = \hbar\omega_\alpha|\alpha\rangle, \qquad \alpha = a, b, s, \tag{2}$$

and the interaction Hamiltonian in the dipole approximation is expressed as

$$H' = -\hat{\mu} \cdot E(t), \tag{3}$$

$$E(t) = E_{\mathrm{IR}}(t)\mathrm{e}^{-\mathrm{i}\hbar\omega_{\mathrm{IR}}t} + E_{\mathrm{VIS}}(t - t_{\mathrm{d}})\mathrm{e}^{-\mathrm{i}\hbar\omega_{\mathrm{VIS}}t} + \mathrm{c.c.}, \tag{4}$$

where $\hat{\mu}$ is the dipole operator, $E_{\mathrm{IR/VIS}}(t)$ is the time envelope of the infrared/visible pulsed fields with frequency $\omega_{\mathrm{IR/VIS}}$ and t_{d} is the (possibly non-zero) delay between the two pulses.

The optical properties of the system are reflected in the time-dependent polarization, which can be calculated from the following trace:

$$P(t) = \mathrm{Tr}\{\hat{\mu}\hat{\rho}(t)\}. \tag{5}$$

The equation of motion of the density matrix $\rho(t)$ in the interaction picture reads

$$\frac{\mathrm{d}\tilde{\rho}(t)}{\mathrm{d}t} = -\mathrm{i}[\tilde{H}'(t), \tilde{\rho}(t)], \qquad \tilde{O} = \mathrm{e}^{\mathrm{i}H_0(t-t_0)}\hat{O}\mathrm{e}^{-\mathrm{i}H_0(t-t_0)}. \tag{6}$$

This equation can be solved to yield

$$\tilde{\rho}(t) = \tilde{\rho}(t_0) + \frac{1}{\mathrm{i}}\int_{t_0}^{t} \mathrm{d}t' \, [\tilde{H}'(t'), \tilde{\rho}(t')] \tag{7}$$

Generally, for any three-level system consisting of levels $|a\rangle$, $|b\rangle$ and $|s\rangle$ (such as the ones depicted in figures 3(b) and (c); for the latter of the two, $|s\rangle$ should be replaced by $|c\rangle$), the general form of $\tilde{\rho}(t)$ reads

$$\tilde{\rho}(t) = \begin{pmatrix} \tilde{\rho}(t)_{aa} & \tilde{\rho}(t)_{ab} & \tilde{\rho}(t)_{as} \\ \tilde{\rho}(t)_{ba} & \tilde{\rho}(t)_{bb} & \tilde{\rho}(t)_{bs} \\ \tilde{\rho}(t)_{sa} & \tilde{\rho}(t)_{sb} & \tilde{\rho}(t)_{ss} \end{pmatrix}, \tag{8}$$

and the induced polarization is given by

$$P(t) = \left\{ \tilde{\mu}_{ba}(t)\tilde{\rho}_{ab}(t) + \sum_{s} \{\tilde{\mu}_{as}(t)\tilde{\rho}_{sa}(t) + \tilde{\mu}_{sb}(t)\tilde{\rho}_{bs}(t)\} \right\} + \mathrm{c.c.}, \tag{9}$$

where $\tilde{\mu}_{ij}(t)$ denotes the dipole transition matrix elements evaluated in the interaction picture defined in equation (6), and the summation is over all possible electronic states s.

For some applications, equation (6) must be solved numerically to obtain $P(t)$, from which the SFG spectrum is readily obtained. Analytical solutions can be obtained for conventional SFG, for which we are interested in second-order non-linear effects and the matrix elements of the density matrix can be solved up to the second order with respect to $E(t)$ to give

$$\begin{aligned} P^{(2)}(t) = -\mathrm{i}\Bigg\{ & \int_{-\infty}^{t} \mathrm{d}t' \sum_{s} \{\tilde{\mu}_{as}(t)\tilde{H}'_{sb}(t')\mathrm{e}^{-(t-t')/T_2^{sa}} - \tilde{\mu}_{sb}(t)\tilde{H}'_{as}(t')\mathrm{e}^{-(t-t')/T_2^{bs}}\}\tilde{\rho}^{(1)}_{ba}(t') \\ & + \int_{-\infty}^{t} \mathrm{d}t' \sum_{s} \{\tilde{\mu}_{sb}(t)\tilde{H}'_{ba}(t')\mathrm{e}^{-(t-t')/T_2^{bs}} \\ & - \tilde{\mu}_{ba}(t)\tilde{H}'_{sb}(t')\mathrm{e}^{-(t-t')/T_2^{ba}}\}\tilde{\rho}^{(1)}_{as}(t') \Bigg\} + \mathrm{c.c.} \end{aligned} \tag{10}$$

in which T_2^{ij} denotes the dephasing time of the transition $j \leftarrow i$. The first term of equation (10) describes a non-linear optical process, in which a coherent vibrational polarization resonantly induced by the short pulse is followed by upconversion: infrared–visible SFG, while the second term is the process inverse to the first one, i.e. difference-frequency generation (DFG).

The Fourier transform of the first term of equation (10), the square of which constitutes the frequency domain SFG signal, is then calculated as

$$\mathcal{P}^{(2)}(\hbar\omega) = \frac{1}{\sqrt{2}}\mathcal{M}(\hbar\omega)\mu_{ba}\rho^{(0)}_{aa}\int \mathrm{d}\hbar\,\omega'\mathcal{E}(\hbar\omega')\frac{1}{\hbar\omega' - \hbar\omega_0 + \mathrm{i}/T_2^{ba}}\mathcal{E}(\hbar\omega - \hbar\omega'), \tag{11}$$

where

$$\mathcal{M}(\hbar\omega) = \sum_s \left(\frac{\mu_{as}\mu_{sb}}{\hbar\omega + \hbar\omega_{as} + \mathrm{i}/T_2^{sa}} - \frac{\mu_{sb}\mu_{as}}{\hbar\omega + \hbar\omega_{sb} + \mathrm{i}/T_2^{sb}} \right) \tag{12}$$

is proportional to the Raman transition moment of the vibrational mode. Here we define $\hbar\omega_{\alpha\beta} = \hbar\omega_\alpha - \hbar\omega_\beta$, $\omega_0 = \omega_b - \omega_a$ is the vibrational frequency and $\mathcal{E}(\hbar\omega)$ is the Fourier transform of $E(t)$ in equation (4). Equation (11) is a general formula for SFG polarization which is valid for arbitrary infrared and visible pulses.

A further approximation can be made by assuming monochromatic infrared and visible fields. In this case, equation (11) is reduced to the well-known formula for vibrationally resonant SFG polarization,

$$\mathcal{P}^{(2)}(\hbar\omega_{\mathrm{sum}} = \hbar\omega_{\mathrm{IR}} + \hbar\omega_{\mathrm{VIS}}) = \chi^{(2)}(\hbar\omega_{\mathrm{sum}}) : E_{\mathrm{IR}}(\hbar\omega_{\mathrm{IR}})E_{\mathrm{VIS}}(\hbar\omega_{\mathrm{VIS}}), \tag{13}$$

where

$$\chi^{(2)}(\hbar\omega_{\mathrm{sum}}) = \frac{1}{\sqrt{2}}\mathcal{M}(\hbar\omega_{\mathrm{sum}})\mu_{ba}\frac{1}{\hbar\omega_{\mathrm{IR}} - \hbar\omega_0 + \mathrm{i}/T_2^{ba}}, \tag{14}$$

is the second-order susceptibility. In order for $\chi^{(2)}(\hbar\omega_{\mathrm{sum}})$ to be non-zero, so that the vibration can be observed using SFG spectroscopy, it is clear that the vibrational mode must be both IR and Raman active (in addition to the requirement that the system must lack a centre of inversion). If the frequency of the visible field is far from any electronic resonances in the system and/or the relaxation of the (virtual) intermediate state is quasi-instantaneous (i.e. with an extremely short T_2^{sa} and T_2^{sb}), the dependence on $\hbar\omega$ of $\mathcal{M}(\hbar\omega)$ can be neglected, and $\chi^{(2)}(\hbar\omega_{\mathrm{sum}})$ represents a purely vibrationally resonant susceptibility. In this case, the three-level system description reduces to a two-level system description, which is then sufficient.

However, when a real resonant electronic excitation occurs in the intermediate state of the SFG processes (figure 3(b)), the possibility of surface enhanced SFG is expected via surface enhanced Raman scattering (SERS) of adsorbates [36]. Recently, two such doubly (infrared and visible) resonant SFG have been demonstrated experimentally for a monolayer of Rhodamine 6G on silica surfaces [37] and CO on Pt(111) [38], and detailed theoretical descriptions for this technique have been developed [39, 40]. This novel type of non-linear spectroscopy is related to IR absorption and Raman scattering, and enables one to explore both the vibrational and electronic resonances of adsorbed molecules, as in a two-dimensional surface spectroscopy. Another type of electronic resonance has been reported recently by Humbert *et al* [41] and Ishibashi and Onishi [11]. The latter observed that the SFG spectra of an octadecanethiol monolayer on a Au substrate exhibits a resonance feature in $\chi^{(2)}_{\mathrm{NR}}$ (in equation (15)) ascribed to a surface electronic excitation in the substrate, associated with an s–d interband transition at 480 nm. These experiments were performed using a two-channel optical parametric amplifier producing a broadband femtosecond infrared pulse and a narrow-band picosecond visible pulse.

The other case where a three-level (or, in the case of an additional electronic resonance, four-level) description is required, is for the situation depicted in (figures 1(c) and/or 3(c)): when the SFG probe pair is preceded by an infrared pump pulse (or when the infrared pulse of the IR–VIS SFG pair is sufficiently powerful itself that it transfers significant population to the first excited state), the second excited state level (and the associated relaxation processes) also has to be taken into account to describe the temporal evolution of the polarization of the system.

Finally, for the situation depicted in figure 1(d), a two-level description suffices, but as the vibrational parameters (frequency and linewidth) are time dependent following the substrate excitation, an analytical expression for the SFG polarization can only be derived

for very specific circumstances [42]; otherwise a numerical solution to the Bloch equations is required [9].

In general, however, the vibrational SFG spectra $I_{\mathrm{SFG}}(\hbar\omega)$ can be reproduced by a simple expression for the second-order non-linear susceptibility consisting of a non-resonant term $\chi^{(2)}_{\mathrm{NR}}$ arising from the surface region of the metal and a resonant term $\chi^{(2)}_{\mathrm{R}} = \chi^{(2)}(\hbar\omega_{\mathrm{sum}})$ of equation (14) associated with the vibrational transition:

$$I_{\mathrm{SFG}}(\hbar\omega) \propto |\chi^{(2)}|^2; \qquad \chi^{(2)} = \chi^{(2)}_{\mathrm{NR}} + \chi^{(2)}_{\mathrm{R}};$$
$$\chi^{(2)}_{\mathrm{NR}} = A_0 \mathrm{e}^{\mathrm{i}\phi}; \qquad \chi^{(2)}_{\mathrm{R}} = \frac{A}{\hbar\omega_{\mathrm{IR}} - \hbar\omega_0 + \mathrm{i}\Gamma}, \tag{15}$$

where the vibrational resonance is described by the resonance frequency $\hbar\omega_0 = \hbar\omega_b - \hbar\omega_a$, linewidth $2\Gamma = 2/T_2$ and constant amplitude A. A_0 is the amplitude of the non-resonant susceptibility and ϕ its phase relative to the vibrational resonance. We can make the connection to conventional IR absorption spectroscopy by noting that the vibrational polarizability is given by

$$\alpha(\hbar\omega_{\mathrm{IR}}) = |\mu_{ba}|^2 \frac{1}{\hbar\omega_0 - \hbar\omega_{\mathrm{IR}} - \mathrm{i}/T_2}. \tag{16}$$

The imaginary part of $\alpha(\hbar\omega_{\mathrm{IR}})$ determines the infrared absorption spectrum $I(\hbar\omega_{\mathrm{IR}})$:

$$I(\hbar\omega_{\mathrm{IR}}) \equiv \mathrm{Im}[\alpha(\hbar\omega)] = \frac{1/T_2}{(\hbar\omega_{\mathrm{IR}} - \hbar\omega_0)^2 + (1/T_2)^2}. \tag{17}$$

Thus, it is apparent that when the experimentally observed SFG spectrum can be described by equation (15), the intrinsic $\chi^{(2)}(\hbar\omega_{\mathrm{sum}})$ is related to the infrared absorption spectrum through $1/T_2|\chi^{(2)}(\hbar\omega_{\mathrm{sum}})|^2 = I(\hbar\omega_{\mathrm{IR}})$.

In the following, we will first present theoretical and experimental results of time-resolved SFG experiments following the scheme of figure 1(b): time-resolved investigations of the free induction decay (FID) of surface vibrations. We will focus on two aspects: (i) the dependence of the signal on the temporal shape of the different input pulses and (ii) the investigation of lineshapes using time domain measurements of the FID. Subsequently, we will present an example of a case where the three-level system description is required: an experimental and theoretical study of vibrational excitation of the C–O stretch vibration of carbon monoxide adsorbed on a Ru(001) surface with ultrashort femtosecond infrared (IR) laser pulses. Broadband IR excitation has been found to lead to the transfer of a significant fraction of the CO molecules to their first and second vibrationally excited states, as exemplified in figure 3(c).

3. Experimental details

The experiments were performed with a femtosecond laser system combined with an ultrahigh vacuum (UHV) chamber. An optical parametric amplifier (TOPAS, Light Conversion) pumped by 1–4 mJ from an amplified Ti:sapphire laser system (800 nm, 120 fs, 400 Hz–1 kHz repetition rate) is used to generate tunable near-IR pulses (signal and idler, ∼1–2.5 μm) in BBO. Mid-IR pulses (2–10 μm) are subsequently generated by difference-frequency mixing (DFG) of the signal and idler in $AgGaS_2$. At a wavelength of about 5 μm fs, IR pulses with energies of typically 15 μJ and a bandwidth of typically 150 cm^{-1} (FWHM) are obtained. The residual 800 nm light after the parametric generation is spectrally narrowed to a bandwidth of typically 4 cm^{-1} using a pulse shaper. The spectral narrowing results in a temporal spread for the 800 nm (VIS) upconversion of roughly 4 ps, as verified by cross-correlation measurements. Time domain FIDs are measured with 120 fs pulses at 800 nm. For the SFG experiments the IR

and VIS pulses are focused onto the surface under investigation under an angle of typically 70° with respect to the surface normal. Typical pulse energies are 4 μJ for the VIS and up to 11 μJ for the IR pulses at the sample (beam waist at focus: 0.3 mm FWHM). The centre frequency of the IR is resonant with the vibration under investigation. The SFG light is dispersed in a spectrometer, and detected using an intensified CCD camera [6, 7]. In the frequency-resolved measurements, this gives the SFG spectrum; for the time domain measurements, the SFG signals are spectrally integrated and measured as a function of the delay between the pulses.

4. Time-resolved SFG and FID-SFG

4.1. The influence of pulse shape

By introducing a time delay, t_d, between the infrared and the visible pulses, one can record the time-resolved SFG intensity, as illustrated in figure 1(b). The inverse transform of $P^{(2)}(\hbar\omega)$ gives the time-dependent SFG polarization

$$\begin{aligned} P^{(2)}(t, t_d) &= iM\mu_{ba} E_{VIS}(t - t_d) \int_{-\infty}^{\infty} dt'\, E_{IR}(t') e^{-(i\hbar\omega_0 + 1/T_2)(t-t')} \\ &= iM\mu_{ba}\rho_{ba}(t) E_{VIS}(t - t_d) e^{-i\hbar\omega_{VIS}t}. \end{aligned} \tag{18}$$

The t_d-dependent SFG polarization in the frequency domain is expressed as

$$P^{(2)}(\hbar\omega_{sum}, t_d) = \chi^{(2)}(\hbar\omega_{sum}) E_{IR}(\hbar\omega_{IR}) E_{VIS}(\hbar\omega_{VIS}, t_d), \tag{19}$$

where E_{IR} and E_{VIS} are the amplitudes of the infrared and visible fields, respectively, which are delayed by time t_d with respect to each other. The TR-SFG spectrum is calculated by

$$I(\hbar\omega_{sum}, t_d) = |P^{(2)}(\hbar\omega_{sum}, t_d)|^2. \tag{20}$$

In order to understand qualitatively how the coherent optical effect manifests itself in the time-resolved SFG spectrum, let us assume a δ-pulse for $E_{IR}(t)$. This gives from equation (18)

$$P^{(2)}(t, t_d) = iM\mu_{ba} E_{IR} e^{-(i\hbar\omega_0 + 1/T_2)t} E_{VIS}(t - t_d)\theta(t). \tag{21}$$

The decay component of $P^{(2)}(t, t_d)$ determines the width of the SFG spectrum obtained by the Fourier transformation of $P^{(2)}(t, t_d)$. In addition to the decay of the vibrational coherence T_2, the temporal profile of $E_{VIS}(t - t_d)$ centred at t_d contributes to the net decay component of $P^{(2)}(t, t_d)$. As schematically illustrated in figure 4 the SFG signal for $t_d < 0$ is created by the decreasing portion of $E_{VIS}(t - t_d)$ at $t = 0$. This results in increase of the effective decay constant of $P^{(2)}(t, t_d)$, and causes the width to be broader than the intrinsic one given by $2/T_2$. On the other hand, for $t_d > 0$, the SFG polarization is created by the increasing portion of $E_{VIS}(t - t_d)$ and the effective decay constant of $P^{(2)}(t, t_d)$ becomes small compared to $1/T_2$. Consequently the SFG spectrum becomes narrower than that determined by $1/T_2$ at positive t_d. In the limit $T_{IR,VIS} \gg T_2$ the linewidth is given by the intrinsic width of $2/T_2$. In this case T_2 cannot be determined by the decay slope of $S(t_d)$ as described below.

Indeed, these statements have been experimentally corroborated: Ishibashi and Onishi [43] have observed that the bandwidths of vibrational bands becomes broader when the picosecond visible pulse arrives at a sample earlier than the femtosecond infrared pulse in SFG spectra of a self-assembled monolayer of octadecanethiol on a Au substrate. Similar phenomena have been observed in the TR-two-photon photoemission (2PPE) spectra associated with image potential states at metal surfaces [44, 45]. Experiments with femtosecond pulses exhibited a strong dependence of the measured linewidth on the pump–probe delay time. Energy-resolved 2PPE spectra were theoretically reproduced using the density matrix method by Boger *et al* [46]. Indeed, the experimentally observed gradual decrease in the linewidth with increasing

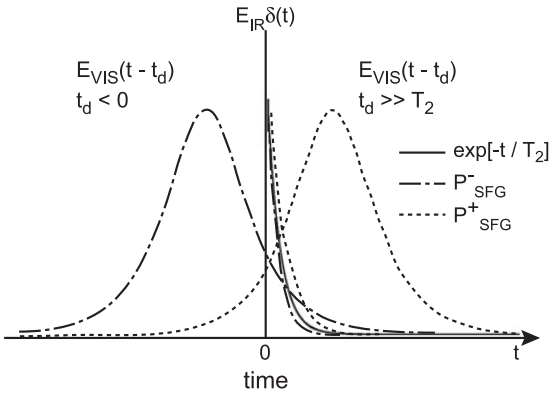

Figure 4. Time envelopes of the visible pulse and the decay of the SFG polarization induced by the δ function IR field at $t = 0$. The solid curve represents the intrinsic SFG polarization decay, $\propto \exp(-t/T_2)$. The dot–dashed and dotted curves are the *effective* SFG polarization decays P^{-}_{SFG} and P^{+}_{SFG} for negative and positive t_{d}, respectively.

pump–probe delay time for the image potential state on Cu(001) could be well reproduced by theory. In addition, it was found that the linewidth depends crucially on the shape of the pump and probe laser pulses.

Another type of time-resolved SFG is the so-called free induction decay (FID) characterized by the dephasing time T_2 $(=2T_1T_2^*/(2T_1+T_2^*))$, where T_2^* is the pure dephasing time and, in the absence of inhomogeneous broadening, $2/T_2$ corresponds to the linewidth observed in the infrared absorption spectrum. In the FID-SFG experiment, a mutually time delayed pair of infrared and visible pulse is used. When the pulses are shorter than the vibrational dephasing time, the infrared pulse creates the vibrational polarization in a coherent manner, and this coherence decays due to dephasing. The delayed visible pulse then creates an SFG signal that probes the remaining coherence at t_{d} so that from the decay of the SFG signal as a function of t_{d}, T_2 can be deduced.

The transient SFG intensity as a function of t_{d} reads

$$S(t_{\mathrm{d}}) = \int_{-\infty}^{\infty} |P^{(2)}(t, t_{\mathrm{d}})|^2 \, \mathrm{d}t, \tag{22}$$

and satisfies the following equation:

$$\frac{\mathrm{d}S(t_{\mathrm{d}})}{\mathrm{d}t_{\mathrm{d}}} = \int_{-\infty}^{\infty} |E_{\mathrm{VIS}}(t - t_{\mathrm{d}})|^2 E_{\mathrm{IR}}(t) \, \mathrm{d}t \times \int_{-\infty}^{t} (E_{\mathrm{IR}}(t') \mathrm{e}^{-(\mathrm{i}(\hbar\omega_0 - \hbar\omega_{\mathrm{IR}}) - T_2^{-1})(t-t')} \, \mathrm{d}t' + \mathrm{c.c.}) - \frac{1}{2T_2} S(t_{\mathrm{d}}). \tag{23}$$

This indicates that the coherent mixing occurs in the overlap between $E_{\mathrm{IR}}(t)$ and $E_{\mathrm{VIS}}(t - t_{\mathrm{d}})$, and causes a shift of the maximum of the SFG intensity from $t_{\mathrm{d}} = 0$ [47]. This shift depends not only on T_2 but also on $T_{\mathrm{IR,VIS}}$. It is also found that the rising edge at negative t_{d} is sensitive to the pulse shapes and gives information on the temporal resolution of the pulses, but is independent of T_2. For t_{d} longer than this overlapping region where the first term of equation (23) vanishes, the SFG intensity simply decays with a time constant T_2 as a function of t_{d},

$$S(t_{\mathrm{d}}) \propto |M\mu_{ba}|^2 \mathrm{e}^{-2t_{\mathrm{d}}/T_2} \theta(t_{\mathrm{d}}). \tag{24}$$

This clearly indicates that T_2 can be determined from the slope of the logarithmic plot of the transient SFG intensity only when the pulse duration is sufficiently shorter than T_2, irrespective of the pulse shape.

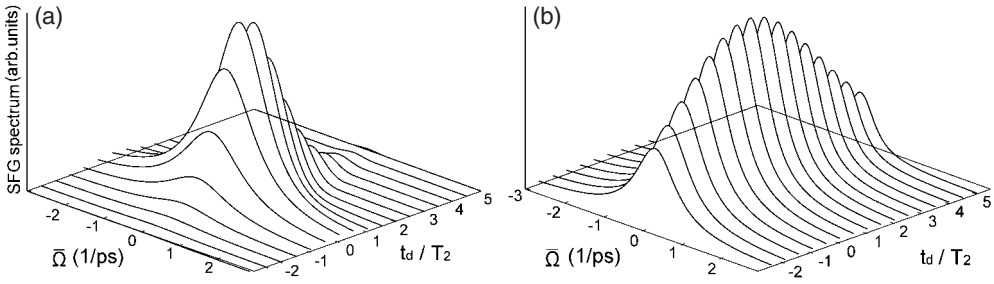

Figure 5. The time-resolved SFG spectrum as a function of the pump–probe delay time t_d at $T_{VIS}/T_2 = 1.0$ and $T_{IR}/T_2 = 0.1$ (a), 3.0 (b).

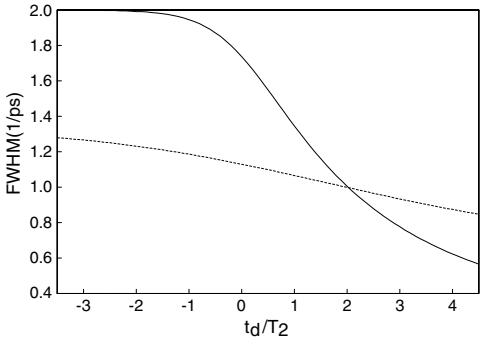

Figure 6. The change of FWHM as a function of the pump–probe delay time t_d for $T_{VIS}/T_2 = 1.0$ and $T_{IR}/T_2 = 0.1$ (solid curve), 3.0 (dotted curve).

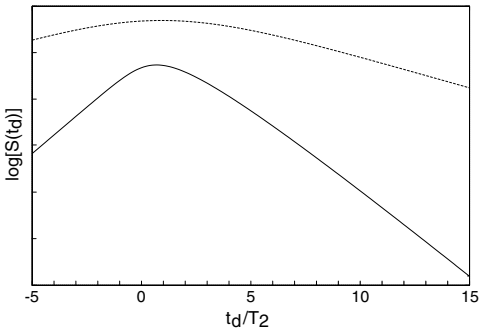

Figure 7. A logarithmic plot of the time-resolved FID-SFG $S(t_d)$ from figure 5.

In the broadband IR-SFG experiment, the typical ranges of the durations of T_{IR} and T_{VIS} are 50–200 fs and 2–10 ps, respectively. Figure 5 shows the evolution of the TR-SFG spectra $I(\hbar\omega_{sum}, t_d)$ calculated using the pulse envelope of $E_{IR,VIS}(t) = E_{IR,VIS}\,\mathrm{sech}(t/T_{IR,VIS})$ as a function of t_d/T_2 for $T_2 = 2$ ps and (a) $T_{IR}/T_2 = 0.1$; $T_{VIS}/T_2 = 1.0$, (b) $T_{IR}/T_2 = 3.0$; $T_{VIS}/T_2 = 1.0$. Clearly, when T_{IR} and T_{VIS} are, respectively, sufficiently shorter and longer than T_2 the FWHM remains unchanged at $2/T_2 = 1/\mathrm{ps}$, being independent of t_d. The Lorentzian SFG spectra centred at $\bar{\Omega} = \omega_{IR} - \omega_0$ gradually grows for negative t_d, and after passing the maximum at a certain point of $t_d > 0$, it decays with decrease in the overlap between the infrared and the visible pulse. The SFG spectra at negative t_d are produced by the overlap between the decaying and growing tails of the visible and infrared pulses, respectively. Figure 6 shows the corresponding changes of the full width at half-maximum (FWHM) obtained from the TR-SFG spectra shown in figure 5. One can easily note that the broad FWHM at negative t_d continues to decrease below $2/T_2$ at large positive t_d, in good agreement with a qualitative explanation of the effective decay time of the induced polarization. A larger T_{IR}/T_2 leads to a smaller deviation of the FWHM from its intrinsic value. The influence of the pulse durations on the TR-SFG spectra manifests itself in the logarithmic plot of the transient behaviour of the time-resolved FID-SFG $S(t_d)$ depicted in figure 7. For $T_{IR}/T_2 = 0.1$ and $T_{VIS}/T_2 = 1.0$, the decay slope at large positive t_d is almost determined by $2/T_2$, while for $T_{IR}/T_2 = 3.0$ and $T_{VIS}/T_2 = 1.0$ the transient behaviour of $S(t_d)$ is predominantly determined by the pulse duration, so no reliable estimate of T_2 is obtained from the decay characteristics of $S(t_d)$.

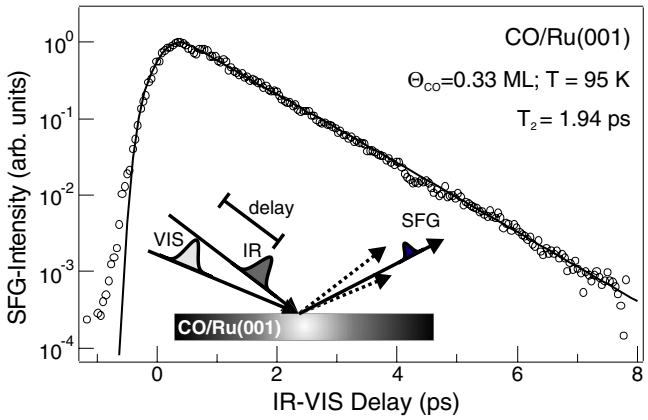

Figure 8. FID-SFG of the C–O stretch vibration of CO on Ru(001) at a temperature of 95 K and a coverage of 0.33 ML. Note a rapid increase of the signal determined by the pulse duration at negative delay (from [34]).

These results (see also [48] for more numerical results using a wider range of parameters T_{IR}/T_2 and T_{VIS}/T_2) indicate that T_2 can be precisely determined from a decay slope of the time-resolved FID-SFG $S(t_{\mathrm{d}})$ at large positive t_{d} observed using pulses sufficiently shorter than T_2. Under this condition, however, the linewidth of the TR-SFG spectrum depends on t_{d} as well as the pulse duration and shape.

As an example of FID-SFG, figure 8 shows the experimental result observed for the C–O stretching mode of CO on Ru(001) at a coverage of 0.33 ML at 95 K [49]. Here the time-resolved measurement of the FID was performed using ultrashort pulses (800 nm, 110 fs $\ll T_2$) for upconversion of the IR polarization. It is noted that for negligible overlap between the infrared and visible pulse, T_2 does not depend on the shape of the pulses. From the exponential decay of the SFG intensity at positive t_{d}, the dephasing time $T_2 = 1.94$ ps (corresponding to a linewidth of $\Gamma = 9.2\ \mathrm{cm}^{-1}$) was determined. An important consequence of this result is that the transient behaviour of the FID can be well described by a single-exponential decay over several orders of magnitude. This indicates a Lorentzian lineshape of the TR-SFG spectra in the frequency domain and therefore a homogeneously broadened spectra given by equation (17). A similar measurement at 340 K resulted in $T_2 = 1.16$ ps. Since T_1 due to electron–hole pair excitation is independent of temperature [16], the difference of T_2 at 95 and 340 K was attributed to the increase of T_2^* due to the anharmonic coupling of the high frequency C–O stretch mode to the low frequency frustrated translational mode [50].

4.2. Lineshape analysis using FIDs

As mentioned in the section above, since the pulse duration (typically ∼100 fs) is appreciably shorter than the decay of the vibrational polarization (dephasing time or inverse linewidth), this decay can be mapped directly in the time domain, in addition to recording the SFG spectrum. Hence, information about the polarization decay can be obtained either by performing a time domain measurement or indirectly from the linewidth in a frequency domain spectrum. These two manners of probing the decay of the macroscopic polarization created by an ultrashort fs infrared pulse are illustrated in figures 1(a) and (b). In a frequency domain measurement the infrared polarization is upconverted using a spectrally narrow (temporally long) visible pulse. The (homogeneous) spectral linewidth (2Γ) is directly related to the vibrational dephasing

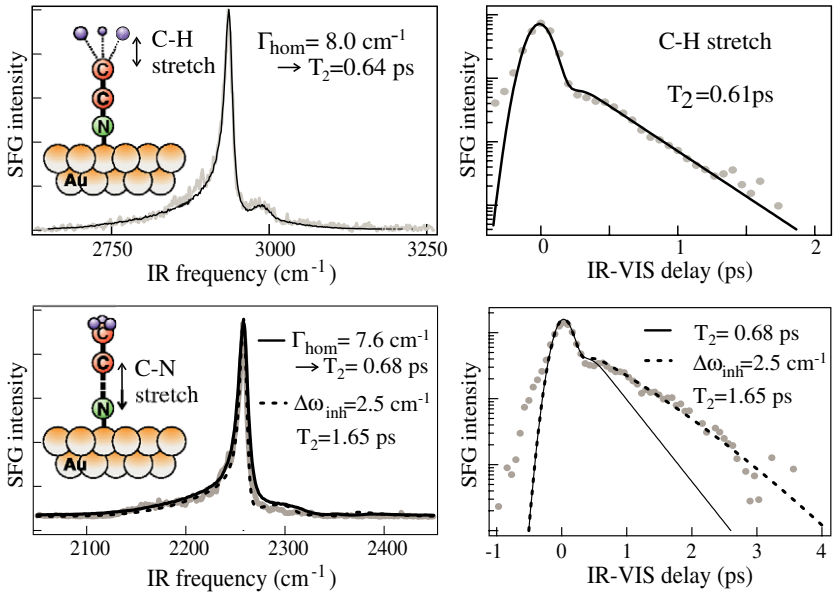

Figure 9. Frequency domain and time domain SFG measurements in the C–N and C–H stretch regions of acetonitrile in contact with a gold surface. Top panels: C–H stretch vibration, in the frequency domain (left), and the time domain. The two data sets are fully consistent, revealing homogeneous behaviour, with an exponential decay corresponding to $T_2 \simeq 0.63$ ps. Bottom panels: C–N stretch vibrations. Whereas the frequency domain data (left) can be described quite satisfactorily in terms of homogeneous behaviour (solid curves), the FID data cannot be described using the same parameters (solid curves). The decay is clearly non-exponential and much slower than expected from the fitted homogeneous linewidth. An inhomogeneous model provides an adequate description of both data sets simultaneously (dashed curves).

time T_2 ($\Gamma = 2/T_2$). In a time domain experiment the polarization is upconverted using a temporally short (spectrally broad) pulse and the integrated SFG intensity is measured as a function of the delay time (t_d) between the infrared and visible pulse. In this way the time evolution of the vibrational polarization (FID) is observed in real time. Since in both schemes the polarization decay is detected, the polarization measured in the time domain is the Fourier transform of the frequency domain result.

Although the two measurement schemes are therefore theoretically equivalent, the time domain experiments are inherently more sensitive to the lineshape as the non-resonant metal response can be separated from the resonant molecular response. We illustrate this with time domain and frequency domain measurements of homogeneously and inhomogeneously distributed oscillators (the C–H and C–N stretch vibrations of liquid acetonitrile (CH_3CN) on an amorphous gold surface). We adapt existing models to elucidate the vibrational decay mechanism and describe both time domain and frequency domain measurements within one formalism.

The upper left panel of figure 9 shows an SFG spectrum in the C–H stretch region of an acetonitrile/gold interface. The main peak from the acetonitrile/gold interface corresponds to the symmetric C–H stretch vibration of the CH_3 stretch vibration of acetonitrile [17]. The measured SFG spectra can be reproduced very well with the calculated SFG intensity ($S_{SFG}(\omega)$) expressed in terms of equation (15). The response of the interface consists of a resonant term ($\chi^{(2)}_{RES}$), to describe the interaction of the light with the vibrational mode, and a non-resonant

term ($\chi^{(2)}_{\mathrm{NR}}$), due to the instantaneous response of the metal to the light. $\chi^{(2)}_{\mathrm{RES}}$ is usually modelled as a Lorentzian response. The non-resonant contribution can be extracted from a SFG spectrum without acetonitrile from the gold/air interface. The solid line through the C–H stretch vibration spectrum is a fit to the data using this model, resulting in $\omega_0 = 2939\ \mathrm{cm}^{-1}$ and $\Gamma = 8.0\ \mathrm{cm}^{-1}$ corresponding to $T_2 = 0.66$ ps.

The upper right panel of figure 9 shows a time domain measurement of the same vibration. This FID consists of both a non-resonant (instantaneous) and a resonant (decaying) contribution. It can immediately be seen that the decay of the resonant signal is exponential, with a slope of 3.2 THz ($=2/T_2$), corresponding to $T_2 = 0.61$ ps, in good agreement with the frequency domain analysis. To reproduce the free induction decay, we follow the procedure first described by Owrutski *et al* [51]. The SFG intensity (S_{SFG}) as a function of delay time (τ_{d}) between the infrared and visible fields can be calculated from the time-dependent polarization $P^{(2)}(t, t_{\mathrm{d}})$ as

$$S_{\mathrm{SFG}}(t_{\mathrm{d}}) = \int_{-\infty}^{\infty} \left| P^{(2)}(t, t_{\mathrm{d}}) \right|^2 \mathrm{d}t, \tag{25}$$

where $P^{(2)}(t, t_{\mathrm{d}})$ which takes into account the non-resonant contribution in the transient SFG intensity given by equation (18) is expressed as

$$P^{(2)}(t, t_{\mathrm{d}}) = \overline{E}_{\mathrm{VIS}}(t - t_{\mathrm{d}}) \left\{ \alpha \int_{-\infty}^{t} \overline{E}_{\mathrm{IR}}(t') \overline{\chi}^{(2)}_{\mathrm{RES}}(t - t')\, \mathrm{d}t' + \beta \overline{E}_{\mathrm{IR}}(t) \mathrm{e}^{\mathrm{i}\phi} \right\} \mathrm{e}^{\mathrm{i}(\omega_{\mathrm{IR}} + \omega_{\mathrm{VIS}})t} + \mathrm{c.c.} \tag{26}$$

The first term in brackets in equation (26) describes the resonant interaction of the infrared field with the adsorbate (with a magnitude α), where $\overline{\chi}^{(2)}_{\mathrm{RES}}(t)$ is the time-dependent envelope of the response of the adsorbate. The second term describes the non-resonant instantaneous response of the gold surface to the infrared field with a magnitude β and a phase difference ϕ with respect to the resonant polarization. $\overline{E}_{\mathrm{IR}}(t)$ and $\overline{E}_{\mathrm{VIS}}(t)$ are the IR and VIS field envelopes. The frequency domain Lorentzian response implies single-exponential decay in the time domain. Indeed using equation (25), with $\overline{\chi}^{(2)}_{\mathrm{RES}}(t) = \mathrm{e}^{-t/T_2}$ and $T_2 = 0.61$ ps, results in excellent agreement between data and model as exemplified by the fit to the FID.

Very contrasting behaviour is observed for the C–N stretch vibration of acetonitrile on gold [17], as is evident from the lower two panels of figure 9, which show the SFG spectrum (lower left panel) and the FID (lower right panel). The C–N stretch spectrum can be reproduced very well with equation (15), setting $\omega_0 = 2250\ \mathrm{cm}^{-1}$ and $\Gamma = 7.6\ \mathrm{cm}^{-1}$ ($T_2 = 0.68$ ps), shown as the dashed curve in the spectrum. As both the SFG spectrum and the FID are measurements of the same polarization, the FID should be described with the time domain equivalent (Fourier transform) of the frequency domain response. However, an exponentially decaying $\overline{\chi}^{(2)}_{\mathrm{RES}}(t)$ and $T_2 = 0.68$ ps (the calculated FID, shown as dashed curve in the lower right panel of figure 9) clearly does not describe the measured FID. Apparently, obtaining a good fit with the commonly employed equation (15) is not a guarantee for homogeneous dephasing behaviour. The clear non-exponential decay of the FID seems to suggest a partially inhomogeneous scenario, in which the resonance frequency is not the same for all molecules but varies with the adsorption site[6].

Following [52–54], such a partially inhomogeneous distribution of adsorption sites can be characterized by a Gaussian distribution, $g(\omega_0')$, of resonance frequencies (ω_0') centred around ω_{inh} with a width $\Delta\omega$, i.e. $g(\omega_0') = \frac{2}{\Delta\omega\sqrt{\pi}} \exp\left(-\frac{(\omega_0' - \omega_{\mathrm{inh}})^2}{(\Delta\omega)^2}\right)$. The time domain resonant

[6] An exponential fit to the TD measurement results in a FD FWHM linewidth of 6.6 cm^{-1}, which is significantly too narrow.

response can then be written as

$$\chi^{(2)}_{\mathrm{RES}}(t) = \sum_{\omega_0'} \chi^{(2)}_{\mathrm{RES}}(t, \omega_0') = \int_0^\infty \mathrm{d}\omega_0'\, g(\omega_0')\mathrm{e}^{-t/T_2}\mathrm{e}^{\mathrm{i}(\omega_0'+\omega_{\mathrm{VIS}})t} + \mathrm{c.c.}$$
$$\equiv \overline{\chi}^{(2)}_{\mathrm{RES}}(t)\cos(\omega_{\mathrm{inh}} + \omega_{\mathrm{VIS}})t \tag{27}$$

which consists of a time-dependent envelope $\overline{\chi}^{(2)}_{\mathrm{RES}}(t)$ and an oscillating frequency $\omega_{\mathrm{inh}} + \omega_{\mathrm{VIS}}$. For the frequency range of interest, the envelope can be approximated by $\overline{\chi}^{(2)}_{\mathrm{RES}}(t) = \mathrm{e}^{-t/T_2}\mathrm{e}^{-t^2(\Delta\omega/2)^2}$, as long as $\frac{\Delta\omega}{\omega_{\mathrm{inh}}} \ll 1$. This is a generalized version of the equations commonly used to fit SFG spectra. The amount of inhomogeneity is determined by the product $\Delta\omega T_2$; $\Delta\omega T_2 \ll 1$ describes a homogeneous scenario (obtained by setting $g(\omega_0') = \delta(\omega_0' - \omega_0)$), whereas $\Delta\omega T_2 \gg 1$ yields a totally inhomogeneous distribution of sites. To obtain the frequency domain polarization, we take the Fourier transform of $P^{(2)}(t, t_{\mathrm{d}} = 0)$ and regard the visible field as a CW field.

Applying equations (25)–(27) to calculate the FID and equation (15) in combination with the Fourier transform of equation (27) to reproduce the spectrum yields the fits in the lower panels of figure 9. Using the same dephasing time ($T_2 = 1.65$ ps) and frequency distribution ($\omega_{\mathrm{inh}} = 2250\ \mathrm{cm}^{-1}$ and $\Delta\omega = 2.8\ \mathrm{cm}^{-1}$, $\Delta\omega T_2 = 0.6$), both the SFG spectrum and the FID can be reproduced very well with one set of parameters. This clearly demonstrates that the time domain allows for a more accurate estimation of T_2 and $\Delta\omega$ than the frequency domain. The errors in the derived values for $\Delta\omega$ and T_2 are determined by the signal-to-noise ratio in the tail of the FID, and amount to $\Delta\omega = 2.8 \pm 1\ \mathrm{cm}^{-1}$ and $T_2 = 1.65 \pm 0.4$ ps. For totally inhomogeneous dephasing behaviour however, the frequency domain spectrum can be decisive, as it should be totally symmetric around ω_{inh}.

Although the SFG spectrum and the FID both map the macroscopic polarization at the surface, the time domain measurement is much more sensitive to the spectral lineshape. It is inherently more sensitive to the molecular response than the frequency domain measurement, since the non-resonant signal is only present when the two short pulses overlap. Thus, for IR–VIS delay >0.5 ps the time domain FID is governed solely by the decay of the resonant polarization. In contrast, the frequency domain SFG spectrum does not give an unobscured image of the resonant polarization, since the molecular polarization *always* interferes with the non-resonant metal response. Therefore, independent of the lineshape model employed, a theoretical description of the frequency domain data will always have one extra parameter, namely the phase difference between the resonant and non-resonant responses. An important lesson from these experiments is that obtaining a good fit for an SFG spectrum assuming a Lorentzian response is not a guarantee for homogeneous dephasing behaviour.

5. Excited state vibrational spectroscopy using SFG

In conventional IR spectroscopy with narrow-band IR light only the $v = 0$–1 fundamental transition of the vibration under investigation is excited, since generally the field strengths are insufficient for saturation spectroscopy. However, with femtosecond lasers with sufficient pulse energy, and owing to the large absorption cross section of, e.g., CO molecules on surfaces, significant amounts (tens per cent) of the CO oscillators can be excited to their first excited state, as schematically depicted in figure 3(c) [10]. Subsequently, SFG can be generated from the $v = 1$–2 ('hot band') transition, which is red-shifted because of the anharmonicity of the CO bond. As the bandwidth of the infrared laser (150 cm^{-1}) well exceeds the vibrational anharmonicity (typically 30 cm^{-1} for surface-bound CO), one can 'climb' to even higher vibrational levels.

5.1. Vibrational ladder climbing

We have investigated the C–O stretch vibration of CO on Ru(001) as a function of the IR energy at 95 K. The upper panel of figure 10 depicts SFG spectra as a function of infrared intensity at a surface coverage of approximately 0.01 monolayers and a temperature of 95 K. The coverage was kept sufficiently low to avoid effects of intermolecular coupling (see below). At low IR energies, a Lorentzian resonance is observed associated with the transition from the ground ($v = 0$) to the first excited ($v = 1$) state. With increasing energy the fundamental transition ($v = 0 \rightarrow 1$) is saturated, and significant population is transferred to the ($v = 1$) state. An additional interaction with the broadband infrared field gives rise to a polarization at the ($v = 1 \rightarrow 2$) transition, from which SFG is generated at a slightly lower frequency due to the anharmonicity of the vibrational potential. This effect exhibits a strong non-linear dependence on the infrared energy (as it is a fourth-order ($\chi^{(4)}$) non-linear optical process; see below), which is obvious from figure 10: with increasing IR power the $v = 1 \rightarrow 2$ hot band of the CO stretch vibration becomes clearly visible at 1961.4 ± 0.3 cm^{-1}, in addition to the fundamental transition at 1990.4 ± 0.1 cm^{-1} which is also observed at lower IR energies. From these values the anharmonicity constant is determined as 13.6 ± 0.36 cm^{-1} [10]. The third resonance around 1938 cm^{-1} arises from two contributions: the $v = 2 \rightarrow 3$ hot band and the fundamental transition of the naturally abundant $^{13}C^{16}O$ in $^{12}C^{16}O$ gas. The SFG spectra $I_{\mathrm{SFG}}(\omega)$ can be reproduced very well by an extension of equation (15) to the case of multi-vibrational transition [10, 55]:

$$I_{\mathrm{SFG}}(\omega) \propto |\chi^{(2)}|^2; \qquad \chi^{(2)} = \chi^{(2)}_{\mathrm{NR}} + \chi^{(2)}_{\mathrm{R}}; \qquad \chi^{(2)}_{\mathrm{R}} = \sum_n \frac{A_n}{\omega_{\mathrm{IR}} - \omega_n + \mathrm{i}\Gamma_n}, \tag{28}$$

where the vibrational resonances are described by their resonance frequencies ω_n, linewidths $2\Gamma_n$ and amplitudes A_n, so the $\chi^{(4)}$ contribution is incorporated in $\chi^{(2)}$. A_0 is the amplitude of the non-resonant susceptibility and ϕ its phase relative to the vibrational resonance. The dotted lines in the upper panel of figure 10 depict the fit to the experimental data using this procedure. The dotted curves in the lower panel show the resonant contribution to the non-linear susceptibility as obtained from the fit.

The resonant contributions to the transient spectra can be calculated from the time-dependent polarization of the ground ($v = 0 \rightarrow 1$) and excited state ($v = 1 \rightarrow 2$) transitions that are related to the off-diagonal elements of the density matrix, as $P(\omega) = \mathrm{e}^{\mathrm{i}\omega_{\mathrm{VIS}}t} \times \mathrm{Tr}(\bar{\rho}\bar{\mu})$. The off-diagonal density matrix elements ρ_{ij} oscillate at $\omega_{ij} \approx \omega_{\mathrm{IR}}$ for near-resonant excitation. In the rotating frame, the equations of motion for the different matrix elements of $\overline{\rho}$ read [32, 56]

$$\dot{\tilde{\rho}}_{00} = -\mathrm{i}V_{01}\tilde{\rho}_{10} + \mathrm{c.c.} + \tilde{\rho}_{11}/T_1^{10}, \tag{29}$$

$$\dot{\tilde{\rho}}_{01} = \mathrm{i}V_{01}(\tilde{\rho}_{00} - \tilde{\rho}_{11}) + \mathrm{i}V_{21}\tilde{\rho}_{02} - \tilde{\rho}_{01}[1/(2T_1^{10}) + 1/T_2^{01} + \mathrm{i}\omega_{01}], \tag{30}$$

$$\dot{\tilde{\rho}}_{11} = -\mathrm{i}V_{12}\tilde{\rho}_{21} + \mathrm{c.c.} + \mathrm{i}V_{01}\tilde{\rho}_{10} + \mathrm{c.c.} - \tilde{\rho}_{11}/T_1^{10} + \tilde{\rho}_{22}/T_1^{21}, \tag{31}$$

$$\dot{\tilde{\rho}}_{12} = \mathrm{i}V_{12}(\tilde{\rho}_{11} - \tilde{\rho}_{22}) - \mathrm{i}V_{10}\tilde{\rho}_{02} - \tilde{\rho}_{12}[1/(2T_1^{10}) + 1/T_2^{12} + \mathrm{i}\omega_{12}], \tag{32}$$

$$\dot{\tilde{\rho}}_{02} = -\mathrm{i}(V_{01}\tilde{\rho}_{12} - V_{12}\tilde{\rho}_{01}) - \tilde{\rho}_{02}[1/T_2^{02} + \mathrm{i}\omega_{02}]. \tag{33}$$

The above equations are the independent equations for the density matrix elements. In addition we have

$$\tilde{\rho}_{22} = 1 - \tilde{\rho}_{00} - \tilde{\rho}_{11}, \tag{34}$$

$$\tilde{\rho}_{10} = \tilde{\rho}_{01}^*, \tag{35}$$

$$\tilde{\rho}_{21} = \tilde{\rho}_{12}^*, \tag{36}$$

$$\tilde{\rho}_{20} = \tilde{\rho}_{20}^*. \tag{37}$$

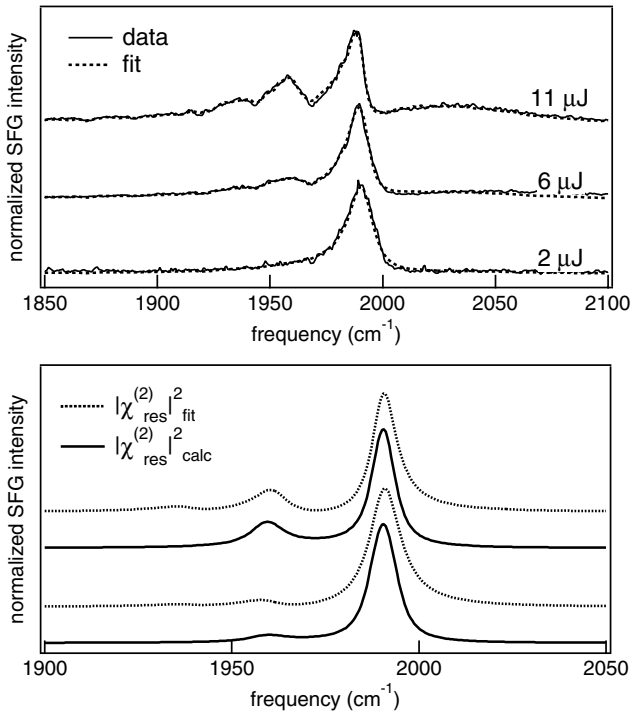

Figure 10. Upper panel: normalized SFG spectra of the stretch of CO on Ru(001) as a function of the IR energy at 95 K (grey curves) together with the least-squares fits to the data (dotted curves) using equation (15). Starting with an IR energy of 11 μJ at a coverage of about 0.007 ML a series of spectra were recorded as a function of decreasing IR energy while dosing with CO via the background. At 11 μJ the fundamental and $v = 1 \rightarrow 2$ hot band transitions are clearly visible. The third resonance is partly due to the $v = 2 \rightarrow 3$ hot band. Lower panel: the resonant part of the fit depicted in the upper panel (dotted curves) and the results of the three-level system calculations (solid curve) described in the text.

In these equations, $\tilde{\rho}_{ij} = \rho_{ij} e^{i(\omega_{ij})t}$, $V_{ij} = -(\mu_{ij}\mathcal{E})/(2\hbar)$, T_1^{ab} and T_2^{ab} denote the population and pure dephasing lifetimes of the transition $a \rightarrow b$, respectively, and the detuning $\omega_{ij} = \omega_{ij} - \omega_{IR}$. μ_{ij} is the transition dipole moment of the transition from i to j and $\mathcal{E}(t)$ the envelope of the incident IR field.

The set of these equations is solved using a fourth-order Runge–Kutta scheme. In these calculations, we set the energy lifetime of the second excited state to be half of the fundamental, i.e. $T_1^{21} = 0.5 \times T_1^{21}$, which follows from wavefunction overlap considerations [57]. We neglect population decay from the second excited state directly to the ground state, since the matrix element associated with this forbidden transition is expected to be very small. Furthermore, we set $\mu_{12} = 2\mu_{01}$, as for a harmonic oscillator, with $\mu_{01} = 2.1 \times 10^{-30}$ C m. The T_2 s are obtained from linewidth measurements of the fundamental (T_2^{01} corresponding to a linewidth of 3 cm^{-1} [50]), hot band transitions (T_2^{12} corresponding to a linewidth of 15 cm^{-1} [10]) and overtone (T_2^{02} corresponding to a linewidth of 6 cm^{-1} [57]) reported previously. Finally, the observed resonant part of the SFG spectrum can be calculated from $I_{res}(\omega) \propto |\chi_{res}^{(2)}|^2 \propto |P(\omega)|^2$, with the polarization $P(\omega) = e^{i\omega_{VIS}t}\,\mathrm{Tr}(\rho\mu) = e^{i\omega_{VIS}t}[(\mu_{01}\rho_{10} - \mu_{10}\rho_{01}) + (\mu_{12}\rho_{21} - \mu_{21}\rho_{12})]$. The first two terms contain the signal at the fundamental transition ω_{01} and the second terms give rise to the signal at ω_{12}, the so-called hot band transition ($v = 1 \rightarrow 2$). Here, we assume that the VIS upconversion pulse is continuous wave.

We account for the spectral width of the upconversion pulse and the instrumental resolution by convoluting the resultant spectra with a 5 cm^{-1} broad Gaussian. Initially, the vibrational lifetime T_1 of both excited states was set to be 2.0 ps in the calculations, as determined from previous time-resolved measurements for CO on other metal surfaces [18, 23], and from extrapolation of the linewidth to 0 K [50].

The SFG light associated with the $v = 1 \rightarrow 2$ hot band transition is due to the interaction of the visible field with the polarization ρ_{12}. It is clear from the above set of equations that the pathway for generating ρ_{12} is $\rho_{00} \rightarrow \rho_{01} \rightarrow \rho_{11} \rightarrow \rho_{12}$, each step comprising one interaction with the incident IR field (note that in the equations (2)–(6) each of these terms has the preceding term multiplied by the infrared field (V) as a source term). Hence, the polarization represented by ρ_{12} is of third order, and the additional interaction with the visible field makes it a fourth-order non-linear optical process. A second pathway leading to ρ_{12} proceeds via the overtone polarization ρ_{02}: $\rho_{00} \rightarrow \rho_{01} \rightarrow \rho_{02} \rightarrow \rho_{12}$. By setting either one of the source terms in equation (5), i.e. $iV_{12}(\tilde{\rho}_{11} - \tilde{\rho}_{22})$ or $iV_{10}\tilde{\rho}_{02}$, to zero, it is possible to distinguish between the relative contributions of the two pathways. It turns out that the contribution via the overtone polarization ρ_{02} amounts to only 1% of the overall ρ_{12}; the pathway via population in $v = 1(\rho_{11})$ is dominant.

The calculated resonant contributions to the spectra in figure 10 are shown as solid lines in the lower panel, and the agreements with results from the fit to the resonant SFG (dotted lines) are excellent. The time-dependent envelopes of the polarization at the fundamental (P_{01}) and the hot band (P_{12}) transition are depicted in the upper panel of figure 11 for the calculation that reproduces the 11 μJ-experiment. The lower panel depicts the time evolution of the population in the first and second excited states. Note that, as expected, the rise of the polarization at the hot band transition P_{12} is delayed with respect to that of the fundamental P_{01}; this is due to the fact that the build-up of the polarization P_{12} arises from a sequence of interactions with the electromagnetic field: the initial interaction creates polarization P_{01}, and subsequently an additional interaction causes population to be transferred to $v = 1$. The third interaction with the IR field gives rise to P_{12}. The final, non-resonant interaction with the visible field creates the SFG from this vibrational polarization. For the same reason the increase of the population in $v = 2$ is delayed with respect to the population increase in the first excited state (lower panel of figure 11). Approximately 15% of the CO molecules are excited to the first vibrationally excited state, and about 5% to the second vibrationally excited state. The relatively large amount of population in $v = 2$ is due to the larger transition dipole moment associated with the $1 \rightarrow 2$ transition compared to the fundamental.

Summarizing, these results demonstrate that, using this saturation SFG technique, excited state vibrational lines can be observed that are inaccessible otherwise. Using the theoretical description presented here allows one to derive from the SFG spectra the vibrational parameters that determine these vibrations (central frequency and linewidth), and investigate, for instance, the mechanism of vibrational dephasing for excited states through the temperature dependence of the excited state linewidth [58].

6. Summary and outlook

A generalized theory of frequency- and time-resolved vibrational sum-frequency generation (SFG) spectroscopy of adsorbates at surfaces is presented using the density matrix formalism. Our theoretical treatment is specifically aimed at addressing issues that accompany the relatively novel SFG approach using broadband infrared pulses. The ultrashort duration of these pulses makes them ideally suited for time-resolved investigations, for which we present a complete theoretical treatment. A second key characteristic of these pulses is their large bandwidth and high intensity, which allow for highly non-linear effects, including

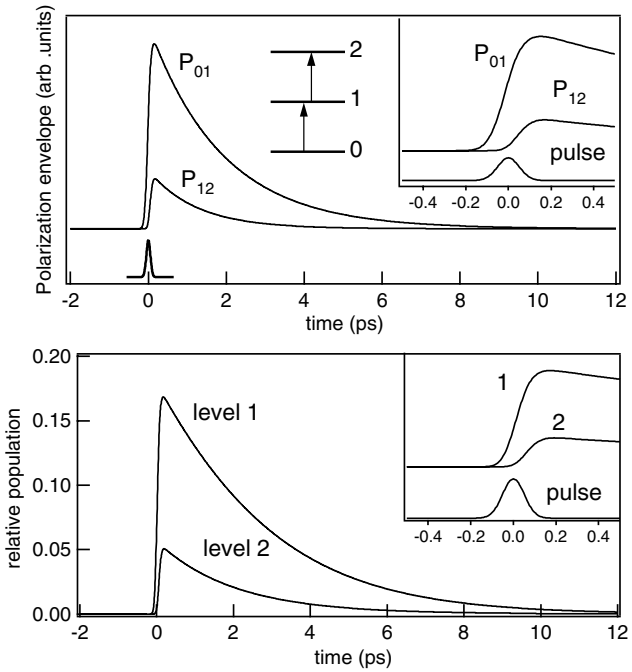

Figure 11. Upper panel: the time evolution of the polarization at the fundamental (P_{01}) and hot band (P_{12}) transitions. These calculations correspond to the 11 μJ data of figure 1. The insets depict the same data around time zero. Note the delayed rise of P_{12} compared to P_{01}. The pulse envelope is depicted around zero delay. Lower panel: the time evolution of the excited state population in the first and second excited state levels.

vibrational ladder climbing of surface vibrations. We derive general expressions relating the density matrix to SFG spectra, and apply these expressions to specific experimental results by solving the coupled optical Bloch equations of the density matrix elements. Thus, we can theoretically reproduce recent experimentally demonstrated hot band SFG spectra using femtosecond broadband infrared excitation of carbon monoxide (CO) on a Ru(001) surface.

In all likelihood, broadband SFG spectroscopy will find an increasing number of applications in a variety of fields. Specific experiments will presumably include additional time-resolved experiments, aimed at directly determining vibrational lifetimes of molecular vibrations at surfaces and the spectroscopic determination of transient surface species, such as reaction intermediates and transition states. In addition, the application of time-resolved SFG for surfaces under ambient conditions, such as liquid interfaces and biological surfaces, will allow for the direct investigation of e.g. the reorientational dynamics of specific molecular groups.

Acknowledgments

This work is part of the research programme of the 'Stichting voor Fundamenteel Onderzoek der Materie (FOM)', which is financially supported by the 'Nederlandse Organisatie voor Wetenschappelijk Onderzoek (NWO)'.

References

[1] Shen Y R 1989 *Nature* **337** 519 and references therein
[2] Buck M and Himmelhaus M 2001 *J. Vac. Sci. Technol.* A **19** 2712
[3] Belkin M A, Shen Y R and Harris R A 2004 *J. Chem. Phys.* **120** 10118

[4] Caudano Y, Silien C, Humbert C, Dreesen L, Mani A A, Peremans A and Thiry P A 2003 *J. Electron. Spectrosc. Relat. Phenom.* **129** 139
[5] Nishi N, Hobara D, Yamamoto M and Kakiuchi T 2003 *J. Chem. Phys.* **118** 1904
[6] van der Ham E W M, Vrehen Q H F and Eliel E R 1996 *Opt. Lett.* **21** 1448
[7] Richter L J, Petralli-Mallow T P and Stephenson J C 1998 *Opt. Lett.* **23** 1594
[8] Star D, Kikteva T and Leach G W 1999 *J. Chem. Phys.* **111** 14
[9] Bonn M, Hess Ch, Funk S, Miners J H, Persson B N J, Wolf M and Ertl G 2000 *Phys. Rev. Lett.* **84** 4653
[10] Hess Ch, Bonn M, Funk S and Wolf M 2000 *Chem. Phys. Lett.* **325** 139
[11] Ishibashi T and Onishi H 2002 *Appl. Phys. Lett.* **81** 1338
[12] Hommel E L and Allen H C 2001 *Anal. Sci.* **17** 137
[13] Symonds J P R, Arnolds H, Zhang V, Fukutani L K and King D A 2004 *J. Chem. Phys.* **120** 7158
[14] Arnolds H, Symonds J P R, Zhang V and King D A 2003 *Rev. Sci. Instrum.* **74** 3943
[15] Fournier F, Zheng W, Carrez S, Dubost H and Bourguignon B 2004 *Phys. Rev. Lett.* **92** 216102
[16] Ueba H 1997 *Prog. Surf. Sci.* **55** 115
[17] Roke S, Kleyn A W and Bonn M 2003 *Chem. Phys. Lett.* **370** 227
[18] Morin M, Levinos N J and Harris A L 1992 *J. Chem. Phys.* **96** 3950
[19] Morin M, Jakob P, Levinos N J, Chabal Y J and Harris A L 1992 *J. Chem. Phys.* **96** 6203
[20] Kuhnke K, Morin M, Levinos N J, Chabal Y J and Harris A L 1993 *J. Chem. Phys.* **99** 6114
[21] Harris A L, Rothberg L, Dubois L H, Levinos N J and Dhar L 1990 *Phys. Rev. Lett.* **64** 2086
[22] Beckerle J D, Cavanagh R R, Heilweil E J and Stephenson J C 1990 *Phys. Rev. Lett.* **64** 2090
[23] Beckerle J D, Cavanagh R R, Casassa M P, Heilweil E J and Stephenson J C 1991 *J. Chem. Phys.* **95** 5403
[24] Guyot-Sionnest P, Dumas P, Chabal Y J and Higashi G S 1990 *Phys. Rev. Lett.* **64** 2156
[25] Matranga C and Guyot-Sionnest P 2000 *J. Chem. Phys.* **112** 7615
[26] Germer T A, Stephenson J C, Heilweil E J and Cavanagh R R 1993 *Phys. Rev. Lett.* **71** 3327
[27] Germer T A, Stephenson J C, Heilweil E J and Cavanagh R R 1994 *J. Chem. Phys.* **101** 1704
[28] Culver J P, Li M, Hochstrasser R M and Yodh A G 1996 *Surf. Sci.* **368** 9
[29] Culver J P, Li M, Hochstrasser R M and Yodh A G 1996 *Chem. Phys.* **205** 159
[30] Bandara A, Kubota J, Onda K, Wada A, Domen K and Hirose C 1999 *Surf. Sci.* **435** 83
[31] Domen K, Bandara A, Kubota J, Onda K, Wada A, Kano S and Hirose C 1999 *Surf. Sci.* **428** 349
[32] Harris A L and Rothberg L 1991 *J. Chem. Phys.* **94** 2449
[33] Bonn M, Hess Ch, Roeterdink W G, Ueba H and Wolf M 2004 *Chem. Phys. Lett.* **388** 269
[34] Hess Ch, Wolf M and Bonn M 2000 *Phys. Rev. Lett.* **85** 4341
[35] Bonn M, Hess Ch and Wolf M 2001 *J. Chem. Phys.* **115** 7725
[36] Chang R K and Furtak T E (ed) 1982 *Surface Enhanced Raman Scattering* (New York: Plenum)
[37] Raschke M B, Hayashi M, Lin S H and Shen Y R 2002 *Chem. Phys. Lett.* **359** 367
[38] Chou K C, Westerberg S, Shen Y R, Ross P N and Somorjai G A 2004 *Phys. Rev.* B **69** 153413
[39] Huang J Y and Shen Y R 1994 *Phys. Rev.* A **49** 3973
[40] Hayashi M, Lin S H, Raschke M B and Shen Y R 2002 *J. Phys. Chem.* **106** 2271
[41] Humbert C, Dreesen L, Mani A A, Caudano Y, Lemaire J J, Thiry P A and Peremans A 2002 *Surf. Sci.* **502/503** 203
[42] Roke S, Kleyn A W and Bonn M 2001 *J. Phys. Chem.* A **105** 1683
[43] Ishibashi T and Onishi H 2001 *Chem. Phys. Lett.* **346** 413
[44] Hertel T, Knoesel E, Hotzel A, Wolf M and Ertl G 1997 *J. Vac. Sci. Technol.* A **15** 1503
[45] Shumay I L, Höfer U, Reuß Ch, Thomann U, Wallauer W and Fauster Th 1998 *Phys. Rev.* B **58** 13974
[46] Boger K, Roth M, Weinelt M and Fauster Th 2002 *Phys. Rev.* B **65** 075104
[47] Mii T and Ueba H 1999 *Surf. Sci.* **427/428** 324
[48] Ueba H, Sawabu T and Mii T 2002 *Surf. Sci.* **502/503** 254
[49] Hess Ch, Wolf M, Roke S and Bonn M 2002 *Surf. Sci.* **502/503** 304
[50] Jakob P and Persson B N J 1997 *Phys. Rev.* B **56** 10644
[51] Owrutski J C, Culver J P, Li M, Kim Y R, Sarisky M J, Yeganeh M S, Yodh A G and Hochstrasser R M 1992 *J. Chem. Phys.* **97** 4421
[52] Bain C D, Davies P B, Ong T H, Ward R N and Brown M A 1991 *Langmuir* **7** 1563
[53] Guyot-Sionnest P 1991 *Phys. Rev. Lett.* **66** 1489
[54] van der Voort M, Rella C W, van der Meer L F G, Akimov A V and Dijkhuis J I 2000 *Phys. Rev. Lett.* **84** 1236
[55] Hunt J H, Guyot-Sionnet P and Shen Y R 1987 *Chem. Phys. Lett.* **133** 189
[56] Knoesel E, Hotzel A and Wolf M 1998 *J. Electron. Spectrosc. Relat. Phenom.* **88–91** 577
[57] Jakob P and Persson B N J 1998 *J. Chem. Phys.* **109** 8641
[58] Bonn M, Hess Ch, Roeterdink W G, Ueba H and Wolf M 2004 *Chem. Phys. Lett.* **388** 269